American Journal of Chemistry 2024, 14(2): 13-26
DOI: 10.5923/j.chemistry.20241402.01

Synthesis, Spectroscopic Characterization, X-ray Structural Analysis and Theoretical Calculations of an Ester Derivative of the Coumarin Scaffold: (Coumarin-6-yl)-4-*tert*-Butylbenzoate

Honoré Kouadio Yao[1], Koulabiga Zakaria[2], Akoun Abou[1,*], Abdoulaye Djandé[2], Michel Giorgi[3], Olivier Ouari[4]

[1]Department of Training and Research in Electrical and Electronic Engineering, Research Team: Instrumentation, Image and Spectroscopy, Felix Houphouet-Boigny National Polytechnic Institute, BP 1093 Yamoussoukro, Côte d'Ivoire
[2]Laboratory of Molecular Chemistry and Materials (LC2M), Research Team: Organic Chemistry and Phytochemistry, University Joseph KI-ZERBO, 03 BP 7021 Ouagadougou 03, Burkina Faso
[3]Spectropole, Federation of Chemical Sciences, Marseille FR1739 Campus St. Jérôme, 52 av. Escadrille Normandie-Niemen, 13013 Marseille, France
[4]Institut de Chimie Radicalaire, Equipe SREP, UMR 7273, Université Aix-Marseille, Avenue Escadrille Normandie-Niemen, Service 521, 13397 Marseille Cedex 20, France

Abstract The title compound, C20H18O4 (I), was synthesized by O-acylation of 6-hydroxycoumarin with 4-tert-butylbenzoyl chloride. The compound was characterized with ESI-MS, FT-IR, 1H and 13C NMR spectroscopic analysis. Furthermore the single crystal X-ray structure obtained has C2/c space group and crystallizes in the monoclinic system with dimensions of a = 36.7355 (4) Å , b = 6.8375 (1) Å , and c = 13.6203 (2) Å . In the structure, the planar coumarin ring system and the benzene ring of the benzoate group are almost perpendicular, forming a dihedral angle of 87.22 (8)°. These moieties are linked by the exocyclic ester (-COO-) fragment making a torsion angle of 66.0°. The molecules are associated via C—H···O interactions to form R22(24) dimers which arrange the coumarin moiety into layers nearly parallel to the $(20\bar{2})$ plane. Likewise, the crystal structure is supported by C–H···π and π–π interactions between neighboring rings with centroid–centroid distances less than 3.8 Å . Also, the DFT method was used to minimize the title compound and assess its HOMO and LUMO electron density plots, as well as its molecular electrostatic potentials. Additionally, the HOMO-LUMO energy gap and non-linear optical (NLO) effects were calculated to better understand the molecule's properties. These calculations yield dipole moment, HOMO–LUMO energy gap, polarizability and first-order hyperpolarizability values of 7.71 D, 4.45 eV, 39.2x10-24 and 5.37x10-30 esu, respectively and are compared with those of the urea molecule for the assessment of NLO properties, as well as with the related coumarin derivative 2-oxo-2H-chromen-6-yl-4-methoxybenzoate (II).

Keywords 6-Substituted coumarin derivative, Spectroscopic analysis, Conformational analysis, Quantum chemical calculations

1. Introduction

Coumarin derivatives are one of the important classes of naturally occurring compounds and interest in their chemistry continues because of their usefulness as biologically active agents. The synthesis of coumarin (2-oxo-*2H*-chromene) derivatives has attracted considerable attention of organic and medicinal chemists as these are widely used as fragrances, pharmaceuticals and agrochemicals. They are essential components of many pharmaceutical molecules, including anti-bacterial [1], antioxidant [2], and anti-inflammatory agents [3]. They are also utilized in the perfumery and agrochemical industries as activators and stabilizers [4,5]. Likewise, coumarin derivatives are used in the development of fields such as optical communications, optical computing, dynamic imaging and data storage combined with other desirable properties such as photoswitching. Considerable research into the discovery of new materials with more efficient nonlinear optical (NLO) properties has been carried out experimentally or guided by theoretical calculations to synthesizing more effective photon-manipulating materials

* Corresponding author:
abouakoun@gmail.com (Akoun Abou)
Received: Mar. 11, 2024; Accepted: Apr. 2, 2024; Published: Apr. 17, 2024
Published online at http://journal.sapub.org/chemistry

[6-10]. Among these materials, we can find organic molecules constructed by a donor-acceptor pair linked to a π-delocalized backbone such as coumarin which display attractive NLO properties. These properties can be assessed from their hyperpolarizabilities [6,10,11]. For instance, the first hyperpolarizability provides information about the material's ability to generate second-order nonlinear effects, such as second harmonic generation, sum frequency, and parametric amplification and others [11]. The quantum chemical methods generally used for these theoretical calculations of molecular hyperpolarizabilities values are Hartree-Fock and density functional theories [12-13].

Having in mind the wide variety of their usage and as a continuation of our investigations on hydroxycoumarins acylation products and theoretical calculations [14-15], we report here the synthesis, characterization, crystal structure, geometry optimization, molecular orbital calculations of (coumarin-6-yl)-4-*tert*-butylbenzoate and the resulting results are compared to those of the related coumarin derivative, the 2-oxo-2H- chromen-6-yl 4-methoxybenzoate (II) [16].

2. Experimental and Theoretical Methods

2.1. Synthesis

The following reaction describes an *O*-acylation of 6-hydroxycoumarin with 4-*tert*-butylbenzoyl chloride in the presence of tetrahydrofuran as a solvent and triethylamine as a base.

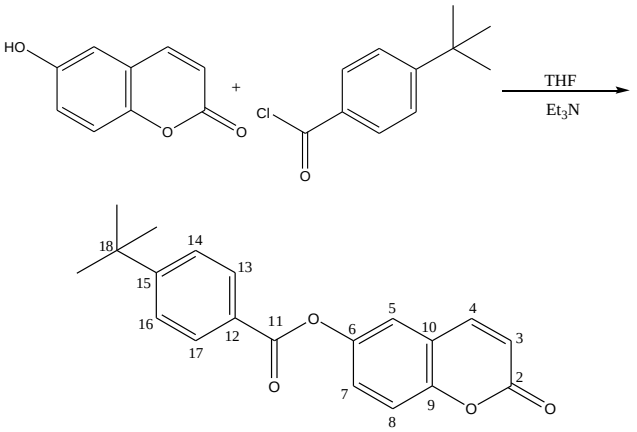

Figure 1. General reaction scheme for the preparation of the title compound

To a solution of 4-tert-butylbenzoyl chloride (1.3 g, 6.17 mmol) in dried tetrahydrofuran (30 mL) was added dried triethylamine (2.6 mL, 18.51mmol) and the substrate 6-hydroxycoumarin (1g, 6.17 mmol) by small portions over 30 min. The mixture was then refluxed for 4 h and poured into 40 mL of chloroform. The solution was acidified with diluted hydrochloric acid 5% until the pH was 2–3. The organic layer was extracted, washed four times with 25 ml of water to neutrality, dried over $MgSO_4$ and the solvent removed. The resulting crude product was filtered off with suction, washed with *n*-hexane and recrystallized from acetone as colorless crystals of the title compound (I). Yield: 91%.

The melting point was measured in open capillaries with a STUART SMP 11 apparatus and is thus uncorrected: m.p. 421–422 K.

2.2. Electrospray Ionization Mass Spectrum

The analyses were carried out with a 3200 QTRAP spectrometer (Applied Biosystems SCIEX) equipped with a pneumatically assisted air pressure ionization (API) source for ESI-MS^+ experiment. The sample in solution was ionized in the following conditions: electrospray tension (ISV): 5500 V; orifice tension (OR): 20 V; nebulizing gas pressure (air): 10 psi. The mass spectra (Figure 2 and 3) were obtained with a quadrupole analyzer.

2.3. ATR-FTIR Spectrum

The Infrared spectrum (Figure 4) was recorded on a Bruker IFS 66/S Fourier Transform Infrared (FTIR) spectrometer, driven by the OPUS 6.5 software and using the ATR (Attenuated Total Reflectance) technique with Germanium tip. The absorption bands in the range 4000-400 are expressed in wavenumber $\bar{\upsilon}$ (cm^{-1}): resolution 1 cm^{-1}, 300 scans.

2.4. NMR Spectra

^1H and ^{13}C-NMR spectra (Figures 5 and 6) were recorded on a Bruker AMX-400 spectrometer at 300 and 100 MHz respectively, using TMS as internal standard (chemical shifts in δ ppm, coupling constants J in Hz) and deuterated chloroform ($CDCl_3$) as a solvent.

The ^{13}C spectrum was obtained from an experience APT (Attached Proton Test).

2.5. Crystal Structure Analysis

Diffraction intensities of the title compound were measured utilizing a mirror monochromator and Cu Kα radiation (λ = 1.54184 Å) at 295 K on a Rigaku Oxford Diffraction SuperNova Dual, Cu to zero, AtlasS2 diffractometer [17]. The structure was determined by direct methods using SIR 2014 [18] and implemented in the WinGX programs [19]. The positional and anisotropic temperature parameters of the heavy atoms, which correspond to 201 crystallographic parameters, were refined utilizing the SHELXL2014 program [20] via a full matrix least squares method.

All hydrogen atoms were fixed geometrically using HFIX geometric constraints [C-H = 0.93 (aromatic) and C-H = 0.96Å (methyl group)] and refined using a riding model with $U_{iso}(H) = 1.2U_{eq}$(C-aromatic) or $1.5U_{eq}$(C-methyl).

The title compound crystallized with disorder in one carbon atom of the *tert*-butyl group. Hence this carbon atom C20 was split over two positions (C20A and C20B) with site occupancies of 0.693 (6) and 0.307 (6), (Table 4). EADP commands in SHELXL were used for the U_{ij} values of equivalent atom pairs of the *tert*-butyl group.

2.6. Computational Procedures

The geometry optimization and some properties such as HOMO–LUMO energy gap, the molecular electrostatic potentials (MEP), the polarizability and the first-order hyperpolarizability of (I) was performed with Opt+Freq method using density functional theory (DFT) combine with restricted exchange correlation functional (RB3LYP) utilizing the 6-311^{++}G(d,p) basis set in ground state. All the theoretical calculations were carried out with GAUSSIAN09 program package [21] using the crystal structure in the solid state as the starting geometry. The results are compared to the related structure, the 2-oxo-*2H*-Chromen-6-yl 4-methoxybenzoate, compound (II), (Figure 8.b) [16].

3. Results and Discussion

3.1. Spectra Analysis

3.1.1. Interpretation of Electrospray Ionization Mass Spectrum

The mass spectrum (Figure 2) displayed two peaks detected at *m/z* 323 and 340 due respectively to the pseudo-molecular ion $[M+H]^+$ and the ammonium adduct $[M+NH_4]^{+,}$ which confirm the molecular weight of 322 g.mol^{-1}, in accordance with the chemical formula $C_{20}H_{18}O_4$.

ESI-MS *m/z* 323 ($[M+H]^+$); 340 ($[M+NH_4]^+$).

ESI-MS/MS *m/z* (%): 323 (MH^+, 81), 161.2 (100), 146.3 (3.17), 105.3 (1.06). (Figure 3)

3.1.2. Infrared Spectrum

For the studied compound, the FTIR spectrum showed absorption bands at 3203.4 cm^{-1} (C-H, aromatic), 2966.1 cm^{-1} (C-H, aliphatic), 1754.2 cm^{-1} and 1728.8 cm^{-1} for the two carbonyls, 1254.2 cm^{-1} (C–O–C, lactone), and 1084.7 cm^{-1} (C–O–C, ester). C=C signals were in the range of 1542.4 cm^{-1} to 1677.9 cm^{-1}, (Figure 4).

3.1.3. ^{1}H-NMR Spectrum

The analysis (chemical shifts and coupling constants) of the ^{1}H NMR spectrum (Figure 5) revealed six signals with five in the range 6-8.5 ppm due to aromatic hydrogens, the nine equivalent methyl protons appeared unambiguously at 1.3 ppm.

^{1}H-NMR ($CDCl_3$, 300 MHz, δ ppm): 1.3 (s, 9H, $3CH_3$); 6.5 (d, 1H, J = 9.6 Hz, H-3); 7.3 (m, 3H, H-5, H-7 and H-8); 7.6 (d, 2H, H-14 and H-16); 7.7 (d, 1H, J = 9.6 Hz, H-4); 8.2 (d, 2H, H-13 and H-17).

3.1.4. ^{13}C (APT)-NMR Spectrum

^{13}C (APT)-NMR sequence provides information on attached protons: CH_3 and CH signals are positive while CH_2 and quaternary carbons signals are negative.

The spectrum of the molecule consisted of 16 signals as expected (Figure 6). Eight positive peaks were observed suggesting the nine aromatic tertiary carbons and the shielded primary carbons of methyl groups, whereas eight peaks were inverted, indicating quaternary carbons (C-2, C-6, C-9, C- 10, C-11, C-12, C-15 and C-18).

^{13}C (APT)-NMR ($CDCl_3$, 100 MHz, δ ppm): 31.2 ($3CH_3$), 35.4 (C-18), 117.6 (C-3), 118.1 (C-5), 119.4 (C-12), 120.5 (C-7), 125.7 (C-8), 125.9 (C-14 and C-16), 126.2 (C-10), 130.3 (C-13 and C-17), 142.9 (C-4), 147.2 (C-9), 151.7 (C-6), 158.1 (C-15), 160.6 (C-2), 165.2 (C-11).

3.1.5. Heteronuclear Single-Quantum Correlation (HSQC) NMR Spectrum

As expected, eight spots were observed in the 2D HSQC-NMR spectrum (Figure 7) providing correlations between the primary carbons and the protons of methyl groups as well as between tertiary carbons (C-3, C-4, C-5, C-7, C-8, C-14 and C-16, C-13 and C-17) and their directly attached proton via the $^1J_{C\text{-}H}$ scalar coupling.

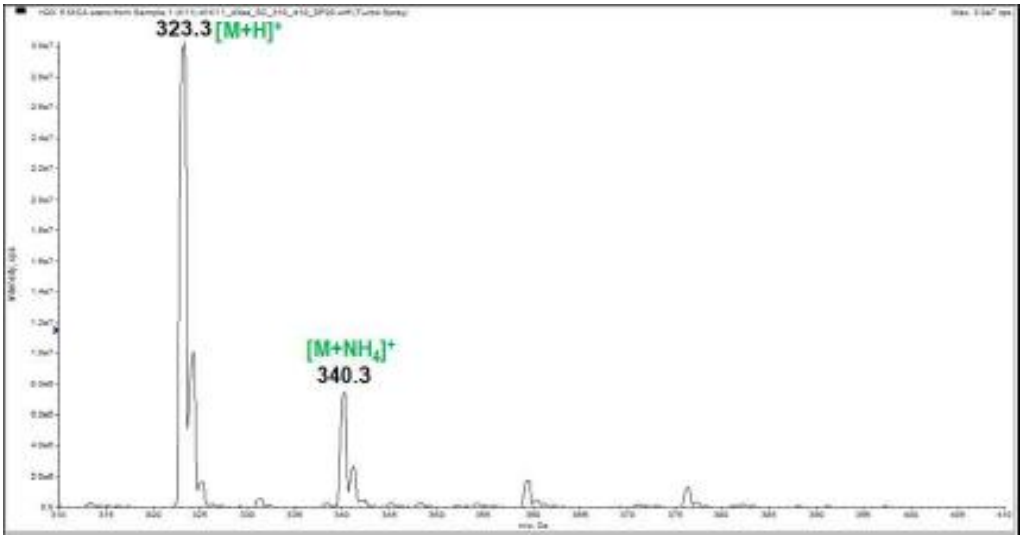

Figure 2. Electrospray ionization mass spectrum of the studied sample

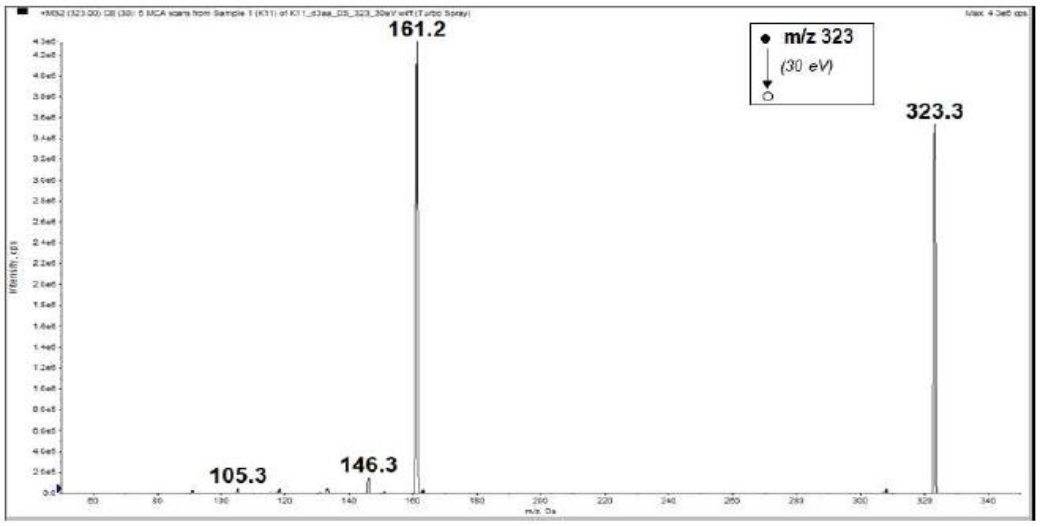

Figure 3. MS/MS spectrum of the protonated molecular ion peak (MH^+) at *m/z* 323

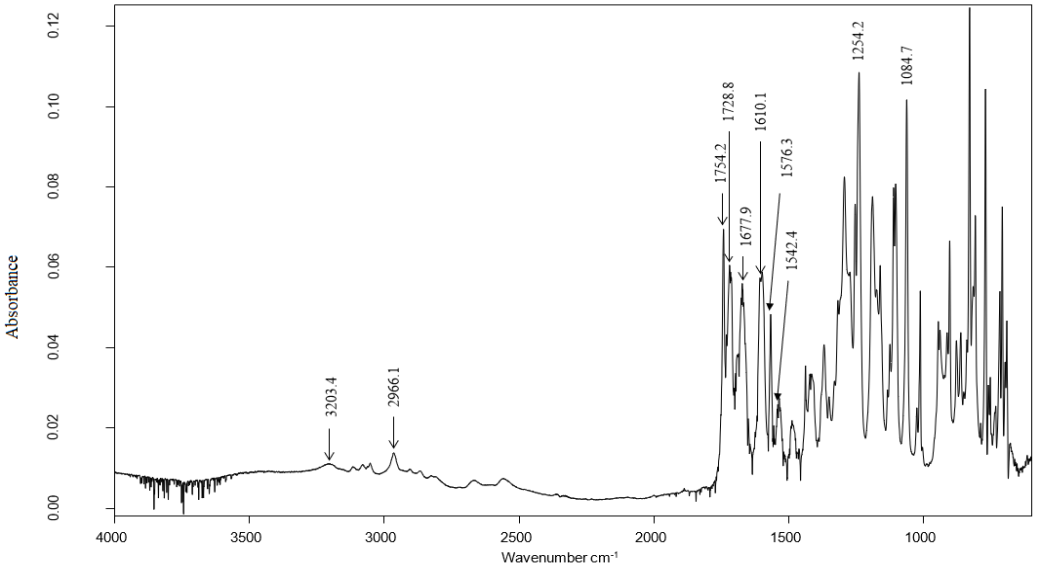

Figure 4. Experimental ATR-FTIR Spectrum

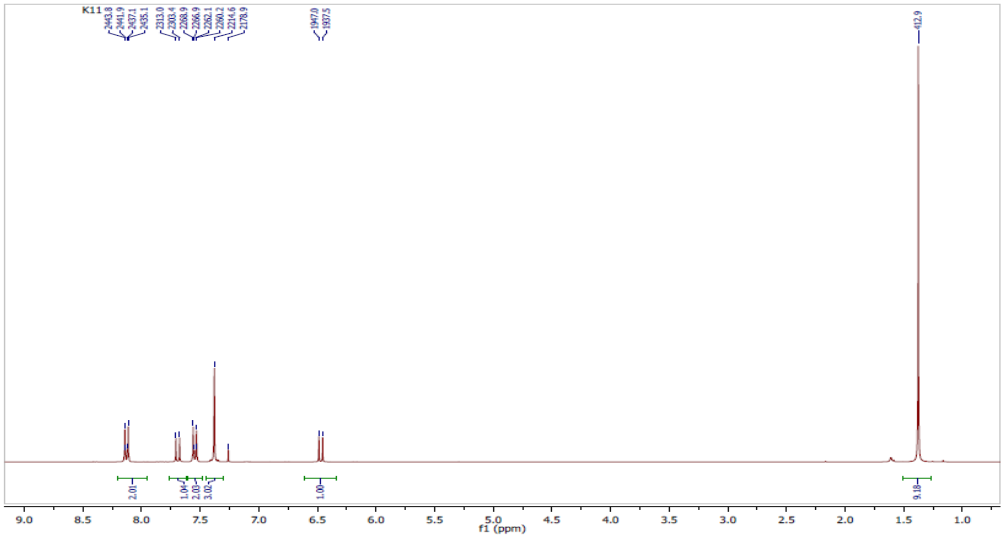

Figure 5. Experimental ^{1}H-NMR Spectrum: $CDCl_3$, 300 MHz

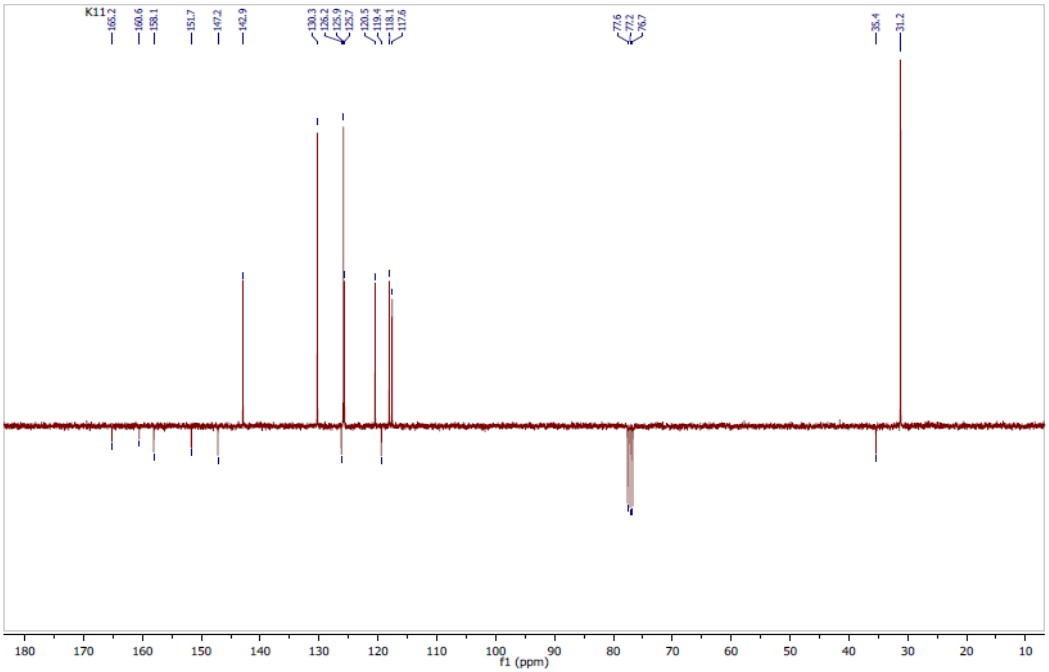

Figure 6. Experimental ^{13}C (APT)-NMR Spectrum: $CDCl_3$, 100 MHz

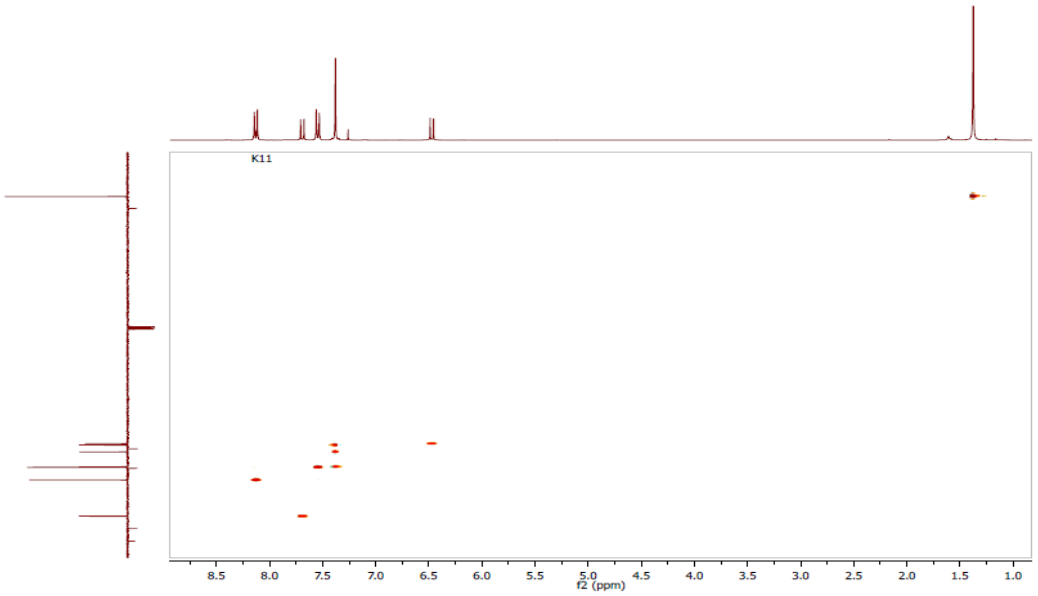

Figure 7. Experimental HSQC Spectrum: $CDCl_3$, ^1H-NMR 300 MHz; ^3C (APT)-NMR 100 MHz

3.1.6. Conclusion of Spectra Analysis

The overlaying of the spectroscopic outcomes originating from the spectral analysis validates the depicted coumarin molecule in Figure 1.

3.2. Structural Description

3.2.1. Structural Commentary

The structure of the coumarin derivative (I) is illustrated in Figure 8.a. In the structure, a methyl group of the *tert*-butyl substituent exhibits a rotational disorder. This group is split over two positions, with refined site-occupation factors of 0.693 (6) and 0.307 (6), Table 4. The planar chromene ring system and the benzene ring of the benzoate group are nearly perpendicular (dihedral angle of 87.22 (8)°). These perpendicular moeties are connected by the exocyclic (-COO-) moiety. An inspection of the bond lengths shows that there is a slight asymmetry of the electronic distribution around the pyrone ring: the C2—C3 [1.340 (3) Å] and C1—C2 [1.441 (1) Å] bond lengths are shorter and longer, respectively, than those expected for a C_{ar}—C_{ar} bond.

This shows that the electron density is weaker in the C2-C3 bond of the pyran-2-one ring, leading to the formation of the double bond, as noticed in other coumarin ester derivatives [22-23].

Table 1. Crystal data and details of the structure determination

chemical formula	$C_{20}H_{18}O_4$	Theta range for data collection [°]	3.3 - 75.8
Formula weight	322.34	Crystal size [mm^3]	0.36× 0.24 × 0.12
Temperature [K]	295	Index ranges	-46 ≤ h ≤46; -8 ≤ k ≤ 8; -13 ≤ l ≤ 16
Wavelength λ [Å]	1.54184	Reflections collected	15143
Crystal system	Monoclinic	Absorption coefficient [mm^{-1}]	0.72
Space group	C2/c	Theta full [°]	67.684
Unit cell dimensions		F(000)	1360
a [Å]	36.7355 (4)	Refinement method	Full-matrix least squares on F^2
b [Å]	6.8375 (1)	Data/restraints/parameters	3107 /0/ 219
c [Å]	13.6203 (2)	Goodness of fit	1.07
α [°]	90	Final R indices [$F^2 > 2.0\ \sigma(F^2)$]	R_1 = 0.060, wR_1= 0.187
β [°]	98.457 (1)	Density calculated [$g.cm^{-3}$]	1.265
γ [°]	90	Independent reflections	3422
Volume [$Å^3$]	3383.93 (8)	R_{int}	0.027
Z	8	R indices (all data)	0.064
Crystal description	Prism	$\Delta\rho_{max}$, $\Delta\rho_{min}$ (e $Å^{-3}$)	0.44, -0.49
crystal color	Colorless	$(\Delta/\sigma)_{max}$	< 0.001
Diffractometer	SuperNova, Dual, Cu at zero, AtlasS2	Absorption correction	multi-scan; CrysAlisPro 1.171.42.79a (Rigaku Oxford Diffraction, 2022) Empirical absorption correction using spherical harmonics, implemented in SCALE3 ABSPACK scaling algorithm.

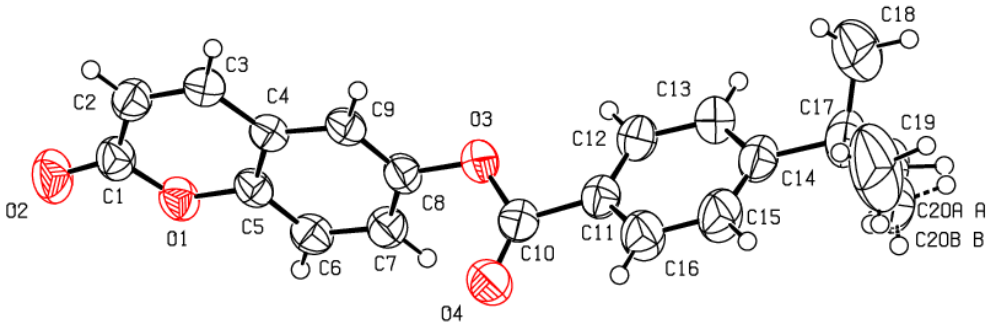

Figure 8.a. An ORTEP view of the title compound (I) with the atomic numbering scheme. Displacement ellipsoids are shown at the 50% probability level

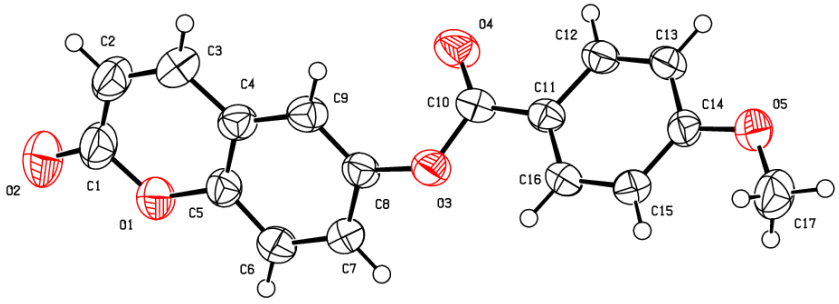

Figure 8.b. An ORTEP view of compound (II) with the atomic numbering scheme for the sake of structural parameters comparison between (I) and (II)

3.2.2. Supramolecular Features

In the crystal, molecules form $R_2^2(24)$ dimeric units via C—H···O interactions that organize the coumarin moiety into layers almost parallel to the (hkl) plane ($20\bar{2}$) with the 4-(*tert*-butyl)benzoate-benzene moiety nearly perpendicular to this plane (figure 9). These dimers are connected to each other by close intermolecular contacts with distances shorter than the sum of the van der Waals radii [C6···C2 (-x,y,-1/2-z) = 3.297 (3)Å , C1···C6 (-x,y,-1/2-z) = 3.342 (3) Å and C4···C4

(-x,y,-1/2-z) = 3.266 (3)Å (figure 9). In addition, C–H···π and π–π stacking interactions between neighbouring coumarin and pyrone or benzene rings with centroid–centroid or H–centroid distances less than 3.8 Å , the maximum regarded as suitable for an effective C–H···π or π–π interaction [24], are also present and linked the dimers (fig.9), (Tables 2 and 3). All of the molecular interactions contribute to the stable assembly of the 3D crystals. The perpendicular distances of Cg(I) on ring J and distances between Cg(I) and perpendicular projection of Cg(J) on ring I (slippage) are summarized in Table 3.

Table 2. Hydrogen-bond geometry (Å , °)

D—H…A	D—H	H…A	D…A	D—H…A
C12—H12…O2^{i}	0.93	2.42	3.302(3)	152.2
C7—H7…Cg3^{ii}	0.93	2.88	3.690(2)	147

Symmetry code: (i) −*x*+1, −*y*+1, −*z*+1; (ii) *x*, *y*+1, *z*.

Table 3. Analysis of short ring interactions (Å). Cg1 and Cg2 are the centroids of the pyrone and the benzene fused to pyrone rings, respectively. The distances between the centroid of ring I and its perpendicular projection on ring J, as well as the distances between the centroid of ring I and the perpendicular projection of ring J on ring I (slippage), are reported

Cg(I)	Cg(J)	Symmetry Cg(J)	Cg(I)…Cg(J)	CgI_Perp	CgJ_Perp	Slippage
Cg1	Cg1	-x,y,-1/2-z	3.4542(10)	3.3432 (7)	3.3432 (7)	1.189
Cg2	Cg2	-x,y,-1/2-z	3.4763 (10)	3.2472 (7)	3.2017 (7)	1.354
Cg1	Cg2	-x,2-y,-z	3.6060 (10)	3.3917(7)	3.3343 (7)	1.373
Cg2	Cg2	-x, 2-y, -z	3.6664 (11)	3.3521 (7)	3.3521 (7)	1.485

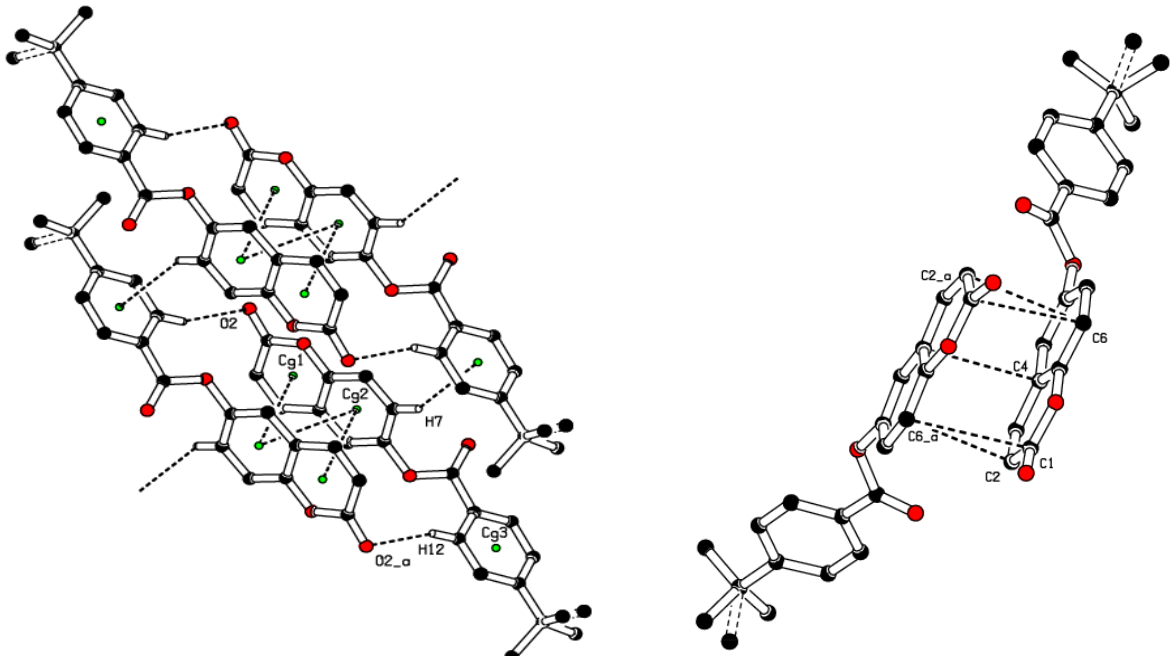

Figure 9. A view of the crystal packing, showing C—H···O hydrogen bonds, C—H···π and π···π stacking interactions connecting molecules into $R_2^2(24)$ dimeric units

Table 4. Fractional atomic coordinates and isotropic or equivalent isotropic displacement parameters (Å ^{2})

Atom	x	y	z	U_{iso}*/U_{eq}	$Occ.(<1)$
O1	0.48578 (4)	0.17294 (18)	0.35844 (10)	0.0565 (4)	
O2	0.43365 (5)	0.0440 (2)	0.28747 (13)	0.0740 (5)	
O3	0.57767 (4)	0.79975 (19)	0.46085 (11)	0.0565 (4)	
O4	0.61611 (4)	0.7330 (2)	0.35045 (12)	0.0677 (4)	
C1	0.44991 (5)	0.1926 (3)	0.31263 (15)	0.0541 (5)	
C2	0.43568 (5)	0.3887 (3)	0.29902 (14)	0.0543 (4)	
C3	0.45665 (5)	0.5461 (3)	0.32483 (13)	0.0485 (4)	
C4	0.49470 (5)	0.5226 (2)	0.36696 (12)	0.0431 (4)	
C5	0.50804 (5)	0.3327 (2)	0.38335 (13)	0.0447 (4)	
C6	0.54398 (5)	0.2958 (3)	0.42419 (14)	0.0504 (4)	

Atom	x	y	z	U_{iso}*/U_{eq}	$Occ.(<1)$
C7	0.56778 (5)	0.4502 (3)	0.44798 (14)	0.0511 (4)	
C8	0.55485 (5)	0.6400 (3)	0.43028 (13)	0.0480 (4)	
C9	0.51912 (5)	0.6782 (2)	0.39134 (13)	0.0458 (4)	
C10	0.60825 (5)	0.8301 (3)	0.41726 (14)	0.0515 (4)	
C11	0.62979 (5)	0.9968 (3)	0.46600 (14)	0.0513 (4)	
C12	0.62638 (5)	1.0556 (3)	0.56130 (15)	00.0555 (5)	
C13	0.64814 (5)	1.2036 (3)	0.60725 (16)	0.0584 (5)	
C14	0.67338 (5)	1.3013 (3)	0.55865 (17)	0.0592 (5)	
C15	0.67551 (7)	1.2448 (4)	0.4617 (2)	0.0752 (7)	
C16	0.65457 (7)	1.0934 (4)	0.41609 (18)	0.0708 (6)	
C17	0.69791 (7)	1.4617 (4)	0.6129 (2)	0.0813 (6)	
C18	0.67516 (11)	1.6003 (5)	0.6661 (3)	0.1228 (14)	
C19	0.71482 (15)	1.5914 (7)	0.5396 (4)	0.163 (2)	
C20A	0.72477 (11)	1.3636 (6)	0.6929 (4))	0.0813 (6)	0.693 (6)
C20B	0.7367 (2)	1.3841 (14)	0.6391 (9)	0.0813 (6)	0.307 (6)
H2	0.411201	0.406584	0.271499	0.065*	
H3	0.446607	0.670742	0.315511	0.058*	
H6	0.552101	0.167872	0.435596	0.060*	
H7	0.592125	0.427746	0.475453	0.061*	
H9	0.511088	0.806565	0.381125	0.055*	
H12	0.609220	0.994703	0.594910	0.067*	
H13	0.645836	1.238377	0.672049	0.070*	
H15	0.691537	1.310883	0.426429	0.090*	
H16	0.657163	1.056442	0.351765	0.085*	
H18A	0.667694	1.535229	0.722300	0.184*	
H18B	0.653759	1.640300	0.621466	0.184*	
H18C	0.689633	1.713215	0.688124	0.184*	
H19A	0.725714	1.704853	0.573649	0.244*	
H19B	0.695967	1.631446	0.487069	0.244*	
H19C	0.733383	1.519191	0.512333	0.244*	
H20A	0.711958	1.320698	0.745520	0.122*	0.693 (6)
H20B	0.743635	1.454997	0.718578	0.122*	0.693 (6)
H20C	0.735760	1.253048	0.665172	0.122*	0.693 (6)
H20D	0.735872	1.249149	0.658101	0.122*	0.307 (6)
H20E	0.749512	1.458398	0.693330	0.122*	0.307 (6)
H20F	0.749405	1.395578	0.582594	0.122*	0.307 (6)

Table 5. Experimental and DFT/ RB3LYP/6-311^{++}G(d,p) calculated bond lengths in (Å) for compounds (I) and (II)

Bond	X-Ray (I)	Calc.(I)	Calc.(II) [14]	Bond	X-Ray	Calc.(I)	Calc.(II) [16]
O1—C5	1.377 (2)	1.364	1.365	C11—C10	1.487 (3)	1.483	1.478
O1—C1	1.379 (2)	1.395	1.395	C7—C8	1.391 (2)	1.398	1.397
O3—C10	1.361 (2)	1.377	1.378	C9—C8	1.367 (3)	1.380	1.383
O3—C8	1.402 (2)	1.395	1.392	C3—C2	1.340 (3)	1.349	1.349
C5—C6	1.378 (3)	1.394	1.392	C1—C2	1.441 (3)	1.459	1.459
C5—C4	1.394 (2)	1.404	1.405	C10—O4	1.196 (2)	1.204	1.205
C4—C9	1.400 (2)	1.405	1.404	C16—C15	1.382 (3)	1.388	1.392
C4—C3	1.440 (2)	1.440	1.441	C12—C13	1.381 (3)	1.391	1.381
C6—C7	1.379 (3)	1.386	1.387	C13—C14	1.387 (3)	1.401	1.404
O2—C1	1.203 (2)	1.202	1.203	C14—C15	1.389 (3)	1.405	1.400
C11—C12	1.382 (3)	1.397	1.405	C14—C17	1.538 (3)	1.537	
C11—C16	1.381 (3)	1.400	1.397				

Table 6. Experimental and DFT/ RB3LYP/6-311^{++}G(d,p) calculated bond angles (°) for compounds (I) and (II)

Bond angle	X-Ray (I)	Calc. (I)	Calc. (II) [14]	Bond angle	X-Ray (I)	Calc. (I)	Calc. (II) [16]
C5—O1—C1	121.84 (14)	122.86	122.8	C8—C9—C4	119.50 (15)	119.80	119.5
C10—O3—C8	118.99 (14)	118.58	120.3	C2—C3—C4	120.13 (16)	120.73	120.7
C6—C5—O1	116.95 (15)	117.51	117.6	O2—C1—O1	116.63 (18)	117.92	117.9
C6—C5—C4	121.88 (16)	121.11	121.0	O2—C1—C2	126.42 (19)	126.22	126.2
O1—C5—C4	121.16 (16)	121.38	121.4	O1—C1—C2	116.95 (15)	115.86	115.9
C5—C4—C9	118.17 (16)	118.76	119.2	O4—C10—O3	123.68 (17)	122.79	123.0
C5—C4—C3	117.74 (15)	117.41	117.3	O4—C10—C11	126.37 (18)	125.58	125.5
C9—C4—C3	124.08 (15)	123.83	123.5	O3—C10—C11	109.95 (16)	111.63	111.5
C5—C6—C7	119.45 (16)	119.42	119.2	C3—C2—C1	121.99 (17)	121.76	121.7
C12—C11—C16	118.73 (18)	118.88	118.9	C9—C8—C7	121.96 (16)	121.07	120.9
C12—C11—C10	119.51 (19)	118.13	118.0	C15—C16—C11	120.0 (2)	120.11	120.9
C16—C11—C10	121.75 (17)	122.97	123.0	C11—C12—C13	120.80 (18)	120.49	120.7
C6—C7—C8	119.02 (17)	119.85	119.6	C14—C15—C16	117.03 (19)	117.29	119.6
C7—C8—O3	117.70 (15)	118.19	116.5	C13—C14—C15	122.0 (2)	121.78	120.0
C9—C8—O3	120.09 (16)	120.63	122.5	C14—C13—C12	121.3 (2)	121.44	120.0

Table 7. Experimental and DFT/ RB3LYP/6-311^{++}G(d,p) calculated dihedral angles (°) for compounds (I) and (II)

Dihedral angles	X-Ray (I)	Calc.(I)	Calc.(II) [14]	Dihedral angles	X-Ray (I)	Calc.(I)	Calc.(II) [16]
C1—O1— C5—C6	-176.73 (15)	179.94	179.9	C9—C8— C7—C6	1.0 (3)	-0.07	0.0
C1—O1— C5—C4	2.7 (3)	0.15	-0.0	O3—C8— C7—C6	175.04 (16)	-176.25	176.3
O1—C5— C4—C9	-178.15 (15)	-179.98	179.8	C4—C3— C2—C1	0.4 (3)	-0.11	0.0
C6—C5— C4—C9	1.3 (3)	0.07	-0.2	O2—C1— C2—C3	-176.3 (2)	-179.84	179.7
O1—C5— C4—C3	1.2 (2)	0.15	-0.2	O1—C1— C2—C3	3.3 (3)	0.11	-0.3
C6—C5— C4—C3	-179.41(16)	-178.92	179.8	C8—O3— C10—O4	3.6 (3)	-1.51	0.4
C8—C9— C4—C5	-0.2 (3)	0.15	0.5	C8—O3— C10—C11	-175.63 (15)	178.55	-179.6
C8—C9— C4—C3	-179.45 (16)	-179.98	-179.5	O4—C10— C11—C16	21.6 (3)	-1.41	179.0
O1—C5— C6—C7	178.19 (16)	179.83	179.8	O3—C10— C11—C16	-159.24 (19)	178.53	-1.0
C4—C5— C6—C7	-1.3 (3)	-0.08	-0.2	O4—C10— C11—C12	-156.9 (2)	178.23	-0.9
C5—O1— C1—O2	174.74 (16)	179.98	0.3	O3—C10— C11—C12	22.3 (2)	1.82	179.1
C5—O1— C1—C2	-4.9 (3)	0.03	0.3	C16—C11— C12—C13	-2.1 (3)	0.23	-0.0
C4—C9— C8—C7	-0.9 (3)	-0.08	-0.4	C10—C11— C12—C13	176.33 (18)	-179.42	179.9
C4—C9— C8—O3	-175.15 (15)	176.18	-176.5	C11—C12— C13—C14	1.7 (3)	-0.16	-0.1
C10—O3— C8—C9	-119.67 (19)	115.11	-53.7	C12—C13— C14—C15	0.5 (3)	-0.06	0.1
C10—O3— C8—C7	66.0 (2)	-168.6	130.1	C12—C11— C16—C15	0.4 (4)	-0.06	0.1
C5—C4— C3—C2	-2.7 (3)	-0.02	0.2	C10—C11— C16—C15	-178.1 (2)	179.59	-179.8
C9—C4— C3—C2	176.59 (17)	-178.88	-179.8	C11—C16— C15—C14	1.9 (4)	-0.16	-0.1
C5—C6— C7—C8	0.1 (3)	0.15	0.3	C13—C14— C15—C16	-2.3 (4)	0.21	-0.0

3.3. Theoretical Calculations

3.3.1. Comparison of Geometrical Parameters

In this work, we compared crystallographic (XRD) and computed structures using three methods. The first two methods are employed to compare geometric parameters, while the third is reserved for Atom-by-atom superimposition of the X-ray structure of (I) on the calculated structure of both structures (I and II, [16]).

The geometrical parameters of (I) and (II) originating from the quantum computations are compared with those obtained from the X-ray crystallographic study in this first approach. An analysis of the calculated bond lengths and bond angles of (I) and comparison with the crystallographic results highlights a good agreement between them, with a root-mean-square deviation (RMSD) of 0.011 Å for bond lengths and 0.7° for bond angles. The latter value is obtained by excluding bond angles involving carbon atoms in the *tert*-butyl group, one of which is disordered (Tables 5 and 6). Also, the inspection of the calculated torsion angles in (I) shows that the benzene ring in the 4-*tert*-butylbenzoate moiety and the coumarin ring system are flat, which agrees with the crystallographic foresight. although the observed O3—C10—C11—C12 and O4—C10—C11—C16 torsion

angles between the benzene ring of the benzoate group and the exocyclic ester side-chain (22.3 (2)°) and (21.6 (2)°), respectively are somewhat larger than the calculated values (1.82°) and (-1.41°) respectively (Table 7). This feature is often observed in 7-substituted coumarin esters. Likewise, an examination of the calculated structure of the related compound namely 2-oxo-*2H*-chromen-6-yl 4-methoxybenzoate (II) in which the 6-substituted fragment i.e 4-methoxybenzoate is also consistent with the crystallographic structure of (I). Indeed, the RMSD used here as an indicator of the accuracy of the prediction errors gives a low value close to zero, i.e. 0.012, indicating a perfect fit to the data.

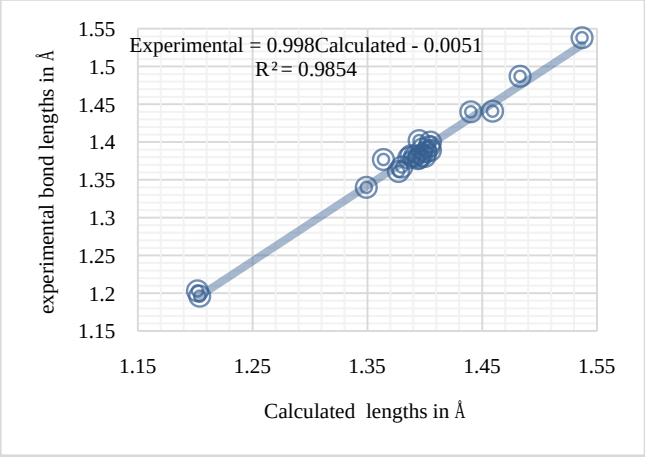

Figure 10. Correlation plot between the experimental and the theoretical bond lengths from (I) (Å)

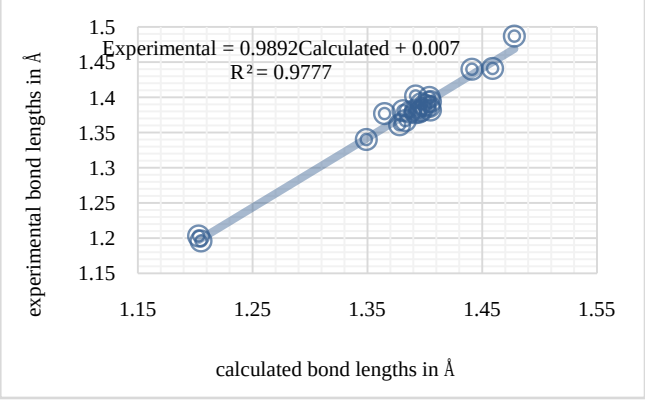

Figure 11. Correlation plot between the experimental bond lengths from (I) and theoretical bond lengths from (II) [16] in (Å)

The second approach involves calculating the correlation coefficients (R^2) between geometrical parameters, such as bond lengths and angles, from the crystallographic study of compound (I) and those of compounds (I) and (II) obtained by quantum calculations, (Tables 5 and 6). The correlation diagrams created in Figures 10 and 11 with regression coefficients R^2 close to unity i.e 0.9854 for (I) and 0.9777 for (II) indicate a strong correlation between experimental bond lengths obtained from X-ray structure determination and those derived from theoretical calculations. Similarly, the graphical representation of experimental bond angles derived from X-ray structural determination of (I) versus calculated bond angles of (I) and (II) yields R^2 values of 0.9502 for compound (I) and 0.8726 for (II) highlights good correlations, Figures 12 and 13.

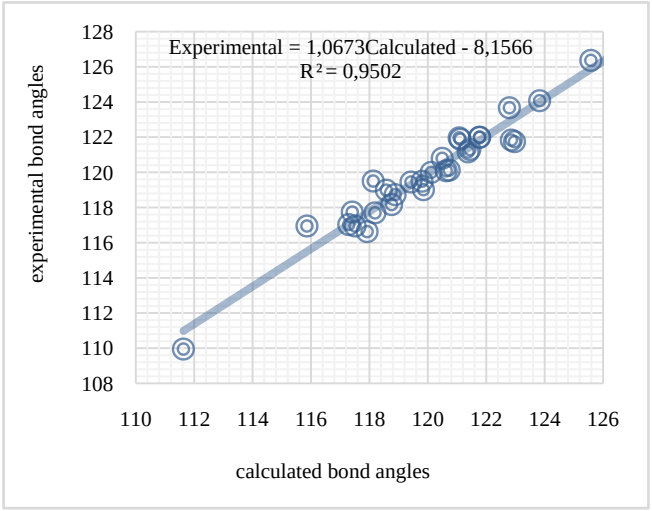

Figure 12. Correlation plot between the experimental and theoretical bond angles frm (I) in (°)

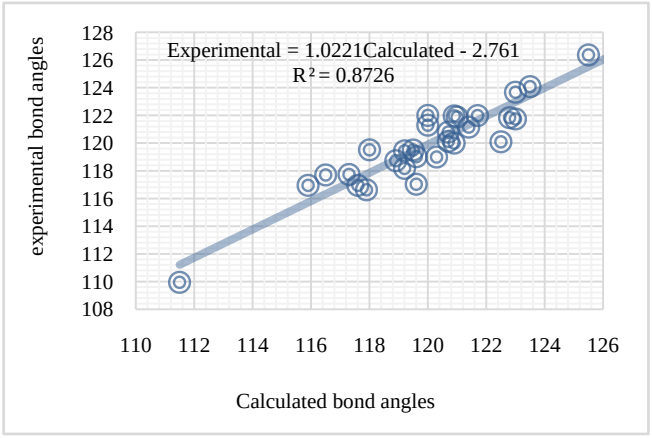

Figure 13. Correlation plot between the experimental bond angles from (I) and theoretical bond angles from (II) [16] in (°)

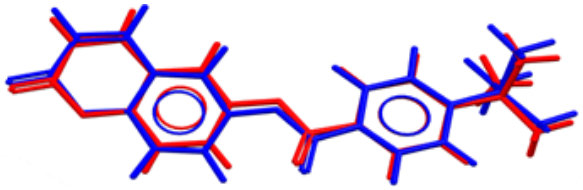

Figure 14. Atom-by-atom superimposition of the X-ray structure (res) on the calculated structure of (I), blue, by (DFT/ B3LYP/6-311^{++}G(d,p)

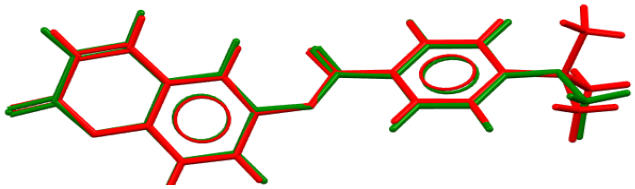

Figure 15. Atom-by-atom superimposition of the X-ray structure (red) on the calculated structure of (II), green, by (DFT/ B3LYP/6-311^{++}G(d,p)

The third comparison method consists of superimposing the molecule obtained by X-ray crystallography and those obtained by quantum chemical calculations utilizing Mercury software [25]. Table 8 shows the RMSD for the superposition and the maximum distance between two equivalent atoms (Max. D).

Table 8. Atom-by-atom overlapping outcomes

		(I)	(II) [14]
X-ray	RMSD	0.21	0.12
	Max. D	0.35	0.31

From the results in Table 8 and Figures 14-15 it can be demonstrated that both models accurately match the XRD structure.

All the above comparisons indicate that the theoretical calculations for (I) and (II) align well with the crystallographic prediction of (I). As (II) also aligns with its own crystallographic structure [16], both calculated structures can be used to assess the chemical properties of these compounds.

3.3.2. Molecular Electrostatic Potential (MEP)

The molecular electrostatic potential (MEP) at a given point P(x,y,z) near a molecule is the force that acts on a positive test charge placed at P through the cloud of electric charge generated at through electrons and nuclei of molecules. Despite the fact that the repartition of the molecular charge remains unchanged thanks to the external test charge (no polarization occurs), the electrostatic potential of a molecule remains a good guide to assess the reactivity of molecules towards positively or negatively charged reactants. So, in this work, MEP is used to illustrate the electronic and nuclear charge distribution which is an appropriate feature for understanding the reactivity of various species [26]. For convenience, the potential, V(r), is written in terms of atomic units (a.u) as the following form [27]:

$$V(r) = \sum_A \frac{Z_A}{|R_A - r|} - \int \frac{\rho(r')d^3r'}{|r' - r|} \quad (1)$$

where Z_A is the charge of nucleus A located at R_A, ρ(r') is the electronic density function of the molecule, and r' is the dummy integration variable.

The results of the calculations of (I) and those of the related structure (II) are shown in color visualizations (Figure 16), where the red color indicates a beneficial area for electrophilic attack (regions of higher negative potential) while the blue color identifies regions of higher positive potential, a favorable area for nucleophilic attack. As can be seen from the figure, there are two possible sites on both compounds for electrophilic attack. These negative regions are localized on the oxygen atoms O2, O3 and O4 with a maximum value of -0.0591 a.u. (I) and -0.05952 a.u. (II), therefore these confirm the existence of the intra-intermolecular C12—H12···O2 (I), C9—H9···O4 and C13—H16···O3 (II) interactions.

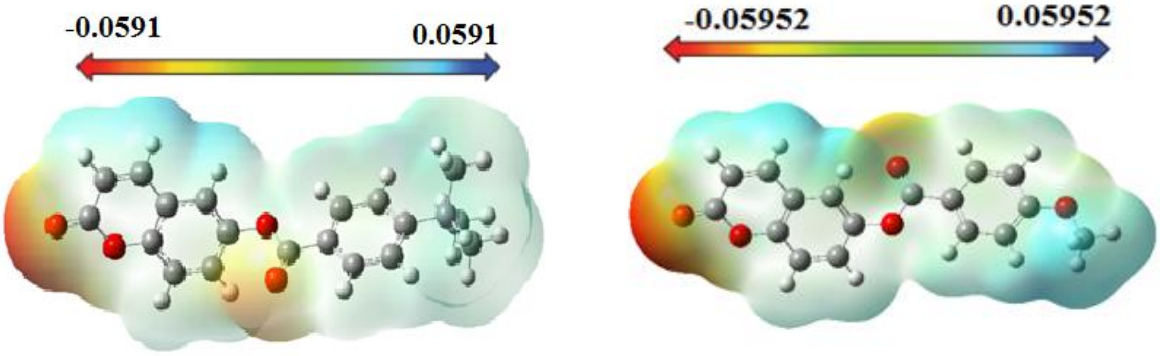

Figure 16. MEP map (in atomic units) calculated using DFT/RB3LYP/6-311++G(d,p)

3.3.3. HOMO-LUMO Analysis

The highest occupied molecular orbital (HOMO) and that of the lowest unoccupied molecular orbital (LUMO) were calculated for the title compound (I) with DFT/RB3LYP/6-311^{++}G(d,p) and the outcomes are depicted in Figure 17. This figure shows that HOMO and LUMO are localized in the plane extending from the coumarin-6-yl moiety linked to the exocyclic ester group (HOMO) to the coumarin-6-yl moiety (LUMO). The calculations also reveal that (I) has 85 occupied molecular orbitals and the value of the energy separation between LUMO and HOMO is 4.45 eV. This large boundary orbital gap and the relative parameters (Table 9) show that (coumarin-6-yl)-4-tert-butylbenzoate is more stable and less chemical reactive and is also called hard molecule [28]. This assertion is corroborated by the absence of negative frequencies in frequency calculation performed by Gaussian. Analysis of the energy gap between the two molecules shows that they are both chemically stable. However, the compound (I) with the higher energy gap is the more chemically stable. Similarly, the highest electrophilicity index value for compound (I) also confirms its greater stability, as this parameter measures energy stabilization when the system acquires additional electronic charge from the environment. Expressions for stability characterization parameters such as energy gap (ΔE), ionization potential (I),

electron affinity (A), absolute electronegativity (χ), absolute hardness (η), softness (S), electrophilicity index (ω), shown in Table 9, are defined as follows [29].

$$\Delta E = E_{LUMO} - E_{HOMO} \quad (2)$$

$$\chi = -\frac{E_{LUMO} + E_{HOMO}}{2} \quad (3)$$

$$\eta = \frac{E_{LUMO} - E_{HOMO}}{2} \quad (4)$$

$$\omega = \frac{\mu^2}{2\eta} \quad (5)$$

$$S = \frac{1}{2\eta} \quad (6)$$

$$I = -E_{HOMO} \quad (7)$$

$$A = -E_{LUMO} \quad (8)$$

$$\mu = -\chi \quad (9)$$

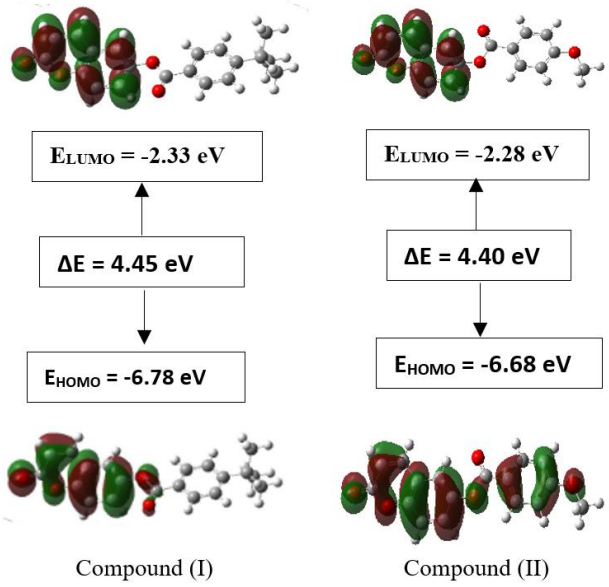

Figure 17. Calculated HOMO and LUMO orbital distributions and energy levels for the molecule (I)

Table 9. The calculated chemical properties of the title compound using DFT/RB3LYP/6-311^{++}G(d,p) levels

	Compound (I)	Compound (II)
E_{LUMO} (eV)	-2.33	-2.28
E_{HOMO} (eV)	-6.78	-6.68
I (eV)	6.78	6.68
A (eV)	2.33	2.28
χ (eV)	4.56	4.48
η (eV)	2.23	2.20
S (eV^{-1})	0.22	0.11
ω (eV)	4.66	4.56
ΔE	4.45	4.40
E (au)	-1074.180	-1031.44

3.3.4. Nonlinear Optical Properties

Nonlinear optical (NLO) effects result from the interactions of electromagnetic fields in various media for produce new fields altered in phase, frequency, amplitude or other characteristics of propagation from incident fields [30]. In recent years, due to the potential applications in modern communication technology, data storage, communication and optical signal processing, a large number of research articles on new materials presenting the effective nonlinear optical properties (NLO) have been of great interest [31-35]. Thus, the use of quantum chemistry methods such as Hartree-Fock (HF) and density functional theory (DFT) for molecular hyperpolarizabilities are currently expected to guide and accelerate the upcoming experimental studies [12,13].

Therefore, in this work, we have used GAUSSIAN-09W to compute the dipole moments (μ), the polarizabilities (<α>), the anisotropy of polarizabilities (<Δα>) and the first-order hyperpolarizabilities (β) which gives information about the ability of the material to generate second-order nonlinear effects [36]. These parameters are defined as follow [37-38]:

$$\mu = \left(\mu_x^2 + \mu_y^2 + \mu_z^2\right)^{\frac{1}{2}} \quad (10)$$

$$\langle\alpha\rangle = \frac{\alpha_{xx} + \alpha_{yy} + \alpha_{zz}}{3} \quad (11)$$

$$\langle\Delta\alpha\rangle = \left[\frac{\left(\alpha_{xx} - \alpha_{yy}\right)^2 + \left(\alpha_{yy} - \alpha_{zz}\right)^2 + (\alpha_{zz} - \alpha_{xx})^2 + 6\left(\alpha_{xy}^2 + \alpha_{xz}^2 + \alpha_{yz}^2\right)}{2}\right]^{\frac{1}{2}} \quad (12)$$

$$\beta = \left[\left(\beta_{xxx} + \beta_{xyy} + \beta_{xzz}\right)^2 + \left(\beta_{yyy} + \beta_{yzz} + \beta_{yxx}\right)^2 + \left(\beta_{zzz} + \beta_{zxx} + \beta_{zyy}\right)^2\right]^{\frac{1}{2}} \quad (13)$$

All the numerical outcomes of the tensors standing for polarizability were converted to the electronic units (esu) and depicted in tables 10, 11 and 12, with (α: 1 a.u. = 0.1482 x10^{-24} esu; β: 1 a.u.= 8.6393x10^{-33} esu), [39].

Table 10. Computation results for the dipole moment (D)

	μ_x	μ_y	μ_z	$<\mu>$
Compound (I)	7.1303	2.9061	-0.3775	7.7091
Compound (II)	7.5628	-1.0578	2.2351	7.9568
urea				1.37

Table 11. All $\alpha \times 10^{-24}$ (esu) components, $<\alpha> \times 10^{-24}$ (esu) and $<\Delta\alpha> \times 10^{-24}$ (esu) values computed using DFT levels of theory

	α_{xx}	α_{xy}	α_{yy}	α_{xz}	α_{yz}	α_{zz}	$<\alpha>$	$<\Delta\alpha>$
Compound (I)	61.17	-0.54	30.94	-1.28	0.49	25.50	39.20	33.39
Compound (II)	56.38	-2.44	28.26	0.49	0.31	19.42	34.69	49.71
urea							3.83	

Table 12. All β (a.u.) components and $\beta \times 10^{-30}$ (esu) values calculated using DFT levels of theory

	β_{xxx} (a.u)	β_{yyy} (a.u)	β_{zzz} (a.u)	β_{xyy} (a.u)	β_{xxy} (a.u)	β_{xxz} (a.u)	β_{xzz} (a.u)	β_{yzz} (a.u)	β_{yyz} (a.u)	β_{xyz} (a.u)	$\beta\times10^{-30}$ (esu)
Compound (I)	590.20	1.83	0.19	38.35	70.82	43.20	-13.05	0.06	-3.50	-30.64	5.37
Compound (II)	591.62	-7.05	-0.26	-0.28	2.27	63.08	-2.04	-2.19	2.15	-31.50	5.12
urea											0.1947

For analysis, urea is one of the prototypical molecules used for comparison purposes in the study of NLO properties of molecular systems. It was frequently used as threshold value of the NLO parameters. As can be seen from tables 10-12, all parameters for compound (I) are higher than those of the urea molecule whose parameters found in the literature are $<\mu> = 1.37$D, $<\alpha> = 3.83\text{x}10^{-24}$ esu [40-41], and $<\beta> = 0.1947\text{x}10^{-30}$ esu [42]. This suggests that (coumarin-6-yl)-4-*tert*-butylbenzoate may have potential applications in the development of NLO materials. In addition, we can also notice from table 10-12 that the title compound has better polarizability and the first-order hyperpolarizability than its related structure, namely 2-oxo-*2H*-chromen-6-yl 4-methoxybenzoate (II).

4. Conclusions

In this work the molecular structure of the title compound (I) was determined via spectroscopic methods and X-ray crystallography. Intermolecular interactions were also analyzed through the Multipurpose Crystallographic Tool Platon [43].

Also, molecular electrostatic potential, HOMO-LUMO analysis and nonlinear optical properties of (coumarin-6-yl)-4-*tert*-butylbenzoate were investigated using DFT/RB3LYP/6-311^{++}G(d,p) calculations. The computed geometric parameters, including bond lengths, bond angles, torsion angles were compared to the corresponding experimental data. The comparison reveals no significant differences between the experimental and theoretical structures, except for the experimental torsion angle, O3—C10—C11—C12 and O4—C10—C11—C16 which differs from the calculated value. The MEP maps indicate that negative potential sites reside on electronegative atoms, and positive potential sites are found around the hydrogen atoms. This information reveals the areas where intra- and intermolecular interactions can occur. Additionally, the estimated first-order hyperpolarizability value which provides information on the material's ability to generate second-order non-linear effects, suggests that both molecules ((I) and (II)) possess non-linear optical properties.

ACKNOWLEDGEMENTS

The authors thank the Spectropole Service of the Federation of Chemical Sciences (Aix-Marseille University, France) for conducting the complete analysis.

REFERENCES

[1] Basanagouda M, Kulkarni M V, Sharma D, Gupta V K, Pranesha P, Sandhyarani P and Rasal V P, *J. Chem. Sci.* (2009); 121: 485–495.

[2] Vuković N, Sukdolak S, Solujić S and Niciforović N, *Arch. Pharm. Res.* (2010); 33: 5–15.

[3] Emmanuel-Giota A A, Fylaktakidou K C, Litinas K E, Nicolaides D N and Hadjipavlou-Litina D J, *Heterocycl. Chem.* (2001); 38: 717–722.

[4] Bauer, K., Garbe, D. & Surburg, H. (1988). Flavors and fragrances. In: Gerhartz, W., Yamamoto, Y. S., Elvers, B., Rounsaville, J. F. & Schulz, G., eds, *Ullmann's Encyclopedia of Industrial Chemistry*, 5th rev. Ed., Vol. A11, New York, VCH Publishers, pp. 208–209.

[5] Boisde, P. M. & Meuly, W. C. (1993). Coumarin. In: Kroschwitz, J. I. & Howe-Grant, M., eds, *Kirk-Othmer Encyclopedia of Chemical Technology*, 4th Ed., Vol. 7, New York, John Wiley, pp. 647–658.

[6] D.R. Kanis, M.A. Ratner, T.J. Marks, *Chem. Rev.* 94 (1994) 195–242.

[7] D.J. Williams, *Thin Solid Films* 216 (1992) 117–122.

[8] P.J. Mendes, J.P. Prates Ramalho, A.J.E. Candeias, M.P. Robalo, M.H. Garcia, *J. Mol. Struct. (Theochem.)* 729 (2005) 109–113.

[9] N.M.F.S.A. Cerqueira, A.M.F. Oliveira-Campos, P.J. Coelho, L.H. Melo de Carvalho, A. Samat, R. Guglielmetti, *Helv. Chim. Acta* 85 (2005) 442–450.

[10] (a) S.P.G. Costa, J. Griffiths, G. Kirsch, A.M.F. Oliveira-Campos, *Ann. Quım. Int. ´* Ed. 94 (1998) 186–188; (b) V.A. Barachevsky, A.M.F. Oliveira-Campos, L.V. Stebunova, G.K. Chudinova, V.G. Avakyan, I.A. Maslianitsin, V.D. Shigorin, *J. Sci. Appl. Photogr. (Russ.)* 47 (2002) 4–8; (c) M.M.M. Raposo, A.M.R.C. Sousa, A.M.C. Fonseca, G. Kirsch, *Tetrahedron* 61 (2005) 8249–8256.

[11] R. Prasad, D.J. Williams, Introduction to Nonlinear Optical Effects in Molecules and Polymers, Wiley-Interscience, New York, 1991.

[12] Y.-X. Sun, Q. L. Hao, W. X. Wei, Z. X Yu, D. D. Lu, X. Wand, and Y. S. Wang. (2009) *J. Mol. Struct. Theochem.*, 904, 74–82.

[13] R. Zhang, B. Du, G. Sun, and Y. Sun. (2010) *Spectrochim. Acta A*, 75, 1115–1124.

[14] Abou A.,Yoda J., Djandé A., Coussan S. and Zoueu T J. *Acta Cryst.* (2018). E74, 761–765.

[15] Abou A., Sosso S., Kouassi A F., Zoueu T J., Djandé A., Ouari O. *Sci. J. Chem.* (*2021); 9(2): 29-44*.

[16] Koulabiga Z., Yao K H., Abou A., Djandé A., Giorgi M., Coussan S. (2024) *Am. J. Org. Chem.*, 12(1): 1-19.

[17] Rigaku OD (2015). *CrysAlis PRO*. Rigaku Oxford Diffraction, Yarnton, England.

[18] Burla M C, Caliandro R, Carrozzini B, Cascarano G L, Cuocci C, Giacovazzo C, Mallamo M, Mazzone A and Polidori G, *J. Appl. Cryst.* (2015), 48: 306–309.

[19] Farrugia L J, *J. Appl. Cryst.* (2012); 45: 849–854.

[20] Sheldrick G M, *Acta Cryst.* (2015); C71: 3–8.

[21] Frisch M. J., Trucks G. W., Schlegel H. B., Scuseria G. E., Robb M. A., Cheeseman J. R., et al.; (2013) GAUSSIAN09. Gaussian, Inc., Wallingford, CT, USA.

[22] Hamdane, D., Lechauve, C., Marden, M.C. and Golinelli-Pimpaneau, B., *Acta Cryst.* (2009). D65, 388–392.

[23] Ziki E, Yoda J, Djandé A, Saba A and Kakou-Yao R, *Acta Cryst.* (2016); E72: 1562–1564.

[24] Janiak J, *J. Chem. Soc. Dalton Trans.* (2000), 3885–3896

[25] Macrae, C.F., Sovago,I., Cottrell, S. J., Galek, P. T. A., McCabe, P., Pidcock, E., Platings, M., Shields, G. P., Stevens, J. S., Towler, M. and Wood, P. A., *J. Appl. Cryst.*, 53, 226-235, 2020.

[26] Politzer P. and J. S. Murray J. S.; (2002) *Theor. Chem. Acc.*, 108(3), 134–142.

[27] Cinar, E. B., Faizi, Md. S. H., Yagci, N. K., Dogan, O. E., Aydin, A. S., Agar, E., Dege, N. & Mashrai, A. (2020). *Acta Cryst.* E76, 1551–1556.

[28] Pearson, R. G. (1986). *Proc. Natl. Acad. Sci. U.S.A.* Nov;. 83(22): 8440-8441.

[29] S. Yazıcı, Ç. Albayrak, I. Gümrükçüoğlu, I. Şenel, and O. Büyükgüngör; (2011) *J. Mol. Struct.*, 985, 292–298.

[30] D. S. Chemia and J. Zyss, *Non LinearOptical Properties of Organic Molecules and Crystal*, Academic Press, New York, NY, USA, 1987.

[31] J. Zyss, *Molecular Non Linear Optics*, Academic Press, Boston, Mass, USA, 1994.

[32] A. Ben Ahmed, H. Feki, Y. Abid, and C. Minot; (2010) *Spectrochim. Acta A*, 75, 1315–1320.

[33] Suponitsky, K.Y., Tafur, S, Masunov A.E.; (2008) *J. Chem. Phys.*, 129, 044109-11.

[34] Avci, D., Başoğlu A., Atalay, Y.; (2011) *Int. J. Quantum Chem.*, 111, 130-147.

[35] A. E.H. Machado., N. M.B. Neto., L. T. Ueno., L. F. de Paula., D.M.S. Araújo., G.S. Oliveira., W.R. Gomes., R. de Paula., P.L. Franzen., S.C. Zilio., A.M.F. Oliveira-Campos., A.M. Fonseca., L.M. Rodrigues., P.O. Nkeonye., R. Hrdina. (2008) *J. Photochem. Photobiol. A* 199, 1, 23–33.

[36] Abraham, J.P., Sajan, D., Hubert, Joe I.H. and Jayakumar, V.S.; (2008) *Spectrochim. Acta A*, 71, 355-367.

[37] Karamanis, P, Pouchan, C. and Maroulis, G.; (2008) *Phys. Rev. A* 77, 013201-013208.

[38] A. Ben Ahmed, H. Feki, Y. Abid, and C. Minot; (2010) *Spectrochim. Acta A*, 75, 1315–1320.

[39] Nkungli, N.K.; Ghogomu, J.N.; (2016) J. *Theor. Chem.*, 2016, 1–19.

[40] Pluta, T.; Sadlej, A.J.; (2001) J. *Chem. Phys.*, 114, 136.

[41] Song, X.; Farwell, S.O.; (2004) *J. Anal. Appl. Pyrolysis*, 71, 901–915.

[42] Eşme, A., Güneşdoğdu Sağdinç, S.; (2014) *BAÜ Fen Bil. Enst. Dergisi Cilt.* 16(1), 47-75.

[43] Spek, A. L., 2009, *Acta Cryst.*, D65, 148–155.